



Full Text View

[Volume 29, Issue 3 \(March 1999\)](#)

Journal of Physical Oceanography

Article: pp. 512–518 | [Abstract](#) | [PDF \(146K\)](#)

Effect of a Western Continental Slope on the Wind-Driven Circulation*

Janet M. Becker

University of Hawaii at Manoa, Honolulu, Hawaii

(Manuscript received September 29, 1997, in final form April 21, 1998)

DOI: 10.1175/1520-0485(1999)029<0512:EOAWCS>2.0.CO;2

ABSTRACT

Numerical solutions of a simple theoretical model of the wind-driven circulation with inertia for a constant density ocean depend strongly upon whether the western boundary is modeled with a vertical sidewall or a smooth continental shelf. In the basin with the continental shelf, unsteady single-gyre inertial solutions are obtained for anticyclonic winds while steady single-gyre inertial solutions typically are obtained for cyclonic winds. In the flat-bottom basin, however, the corresponding model solutions are steady for both anticyclonic and cyclonic winds. In addition, for cyclonic forcing, multiple equilibria are found in the basin with the western continental slope but not in the flat-bottom basin (although the uniqueness of the solutions in the flat-bottom basin has not been proven). The dependence of the model solutions on the topography and the sign of the wind forcing is attributed to the effects of friction, which are localized in the southwest corner of the basin for the continental slope topography, but which are important in boundary layers at vertical sidewalls for the flat-bottom topography.

1. Introduction

Recently, theoretical models of the wind-driven circulation for a homogeneous ocean have been revisited to determine how a western continental slope modifies the classical solutions of [Stommel \(1948\)](#) and [Munk \(1950\)](#) (e.g., [Salmon 1992, 1994](#); [Kubokawa and McWilliams 1996](#)). The motivation for this is two-fold. First, it is well known that the path of the western boundary current is affected by the continental shelf and slope; hence, a better theoretical understanding of how this $O(1)$ topography affects the circulation is warranted. Second, theoretical models of the general circulation have been shown to be sensitive to boundary conditions imposed at coastlines modeled as vertical sidewalls (e.g., [Cummins 1992](#)). As a continental slope acts to direct the flow away from the coast, it is anticipated that this topography will reduce or eliminate the sensitivity of the theoretical models to the sidewall boundary conditions.

Table of Contents:

- [Introduction](#)
- [Dynamics and numerical](#)
- [Numerical solutions](#)
- [Remarks](#)
- [REFERENCES](#)
- [FIGURES](#)

Options:

- [Create Reference](#)
- [Email this Article](#)
- [Add to MyArchive](#)
- [Search AMS Glossary](#)

Search CrossRef for:


- [Articles Citing This Article](#)


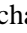
Search Google Scholar for:


- [Janet M. Becker](#)

In the linear approximation, the wind-driven circulation in a basin with a western continental slope is well understood and differs significantly from that in a flat-bottom basin. To see how the linear solution depends upon a western continental slope, consider a homogeneous fluid layer of variable depth governed by the hydrostatic primitive equations. The depth-independent flow in the layer is forced by the wind and is damped by Rayleigh friction. Then, steady linear solutions for the transport streamfunction ψ obey the vorticity equation (e.g., [Welander 1968](#)):







$$J\left(\frac{f}{H}, \psi\right) = R\nabla \cdot \left(\frac{1}{H}\nabla\psi\right) - W \quad (1.1)$$


where $f = \beta y$ is the Coriolis parameter, $H = H(x, y)$ is the fluid depth, $W = W(x, y)$ is the curl of the net stress acting on the fluid (see [section 2](#)), R is the coefficient of Rayleigh friction, and $J(a, b) \equiv a_x b_y - a_y b_x$ is the horizontal Jacobian. The solution of [\(1.1\)](#) also must satisfy $\psi = 0$ at lateral boundaries. We emphasize that the quasigeostrophic approximation has not been made in the derivation of [\(1.1\)](#), which allows us to consider here solutions of [\(1.1\)](#) for which the variation in the fluid depth H is $O(1)$. In particular, we compare solutions of [\(1.1\)](#) for two topographies: (i) a basin with a continental slope that takes the ocean depth H smoothly to zero at the western boundary and bounded at the north and east with vertical sidewalls ([Figs. 1a,b](#) ) and (ii) a flat-bottom basin bounded at the west, north, and east by vertical sidewalls. For both topographies, the southern boundary of the model basin is the equator where the boundary condition $\psi = 0$ corresponds to cross-equatorial symmetry of the dynamics.

[Equation \(1.1\)](#) may be viewed as an advection–diffusion equation for ψ , with “streamlines” f/H and “source” $-W$. Then, lines of constant f/H are characteristics of [\(1.1\)](#) and for the case where the W -forcing term is negligible near boundaries, friction is important where the flow must cross these characteristics to return to the interior. Hence, friction is important where the lines of constant f/H intersect the western boundary. For a flat-bottom ocean with $H(x, y) = \text{const}$, these characteristics are zonal lines and friction is important along the western boundary in the Stommel layer. In contrast, in the basin with a western shelf ([Figs. 1a,b](#) ) , the characteristics intersect the western boundary at the equator ([Fig. 1c](#) ) and the dominant frictional effects are localized in the southwest corner of the basin. We remark that we are not considering here solutions of [\(1.3\)](#) for topographies with closed f/H contours. In these solutions, ψ is advected around the f/H contours and friction acts to diffuse ψ across these closed contours (e.g., [Rhines and Young 1983](#)).

[Figure 2](#)  presents a comparison of the solutions of [\(1.1\)](#) forced by a single-gyre wind stress curl that acts over the middle half of a square basin ($0 \leq x \leq 1, 0 \leq y \leq 1$)

$$W(x, y) = -\sin\left[2\pi\left(y - \frac{1}{4}\right)\right], \quad \frac{1}{4} < y < \frac{3}{4} \quad (1.2)$$

([Fig. 1d](#) ) for the two topographies. That the flow follows the f/H lines is evident in the linear continental slope solution of [Figs. 2a,b](#)  which shows that ψ has a tail that extends toward the southwest, beyond the region of direct wind forcing. This is because the geostrophic contours have been deflected by the continental slope ([Fig. 1c](#) ). The linear flat-bottom solution ([Figs. 2c,d](#) ), however, is confined to the region of direct wind forcing by the zonal geostrophic contours. In addition, the vorticity in the linear continental slope solution ([Fig. 2b](#) ) consists of layers aligned along the f/H contours that are well removed from the western boundary except near the southwest corner of the basin. The vorticity layer of the flat-bottom solution ([Fig. 2d](#) ) is confined to the western boundary and has no direct counterpart in the continental slope solution.

The purpose of the present work is to determine how inertia modifies the linear, single-gyre continental slope solution of [Figs. 2a,b](#)  and to compare these results with the known results for the effects of inertia on the linear flat-bottom solution (e.g., [Veronis 1966](#)). We recognize that baroclinic effects that are not treated here are expected to be significant. These will be the subject of a future study. With inertia, [\(1.1\)](#) becomes (in standard nondimensional form, see [section 2](#))

$$\text{Ro} \frac{\partial \zeta}{\partial t} + J\left(\psi, \frac{\text{Ro}\zeta + y}{H}\right) = -\varepsilon\zeta + W(x, y), \quad (1.3a)$$

where

is the relative vorticity, and $Ro = U/f_0L$ and $\mathcal{E} = R/f_0$ are the Rossby number and nondimensional coefficient of Rayleigh friction, respectively (U/L are velocity/length scales, respectively, and f_0 is a representative value of the Coriolis parameter f). The solutions of (1.3) depend upon the two controlling parameters (Ro, \mathcal{E}).

An effort to determine the effects of inertia on the solutions of (1.3) forced by a double-gyre wind in a basin with a western continental shelf was carried out by [Becker and Salmon \(1997, hereinafter BS97\)](#). They determined numerical solutions of (1.3) in a rectangular basin ($0 \leq x \leq 1, 0 \leq y \leq 2$) forced by the wind stress curl

$$W(x, y) = -\sin \left[2\pi \left(y - \frac{1}{2} \right) \right], \quad \frac{1}{2} < y < \frac{3}{2} \quad (1.4)$$

for two topographies analogous to those considered here: a basin with a western continental shelf and a flat-bottom basin. For fixed values of the Rayleigh friction, steady continental slope solutions were obtained for weak nonlinearity, while above a threshold Rossby number, the continental slope solutions were unsteady with eddies pinching off near the western boundary. BS97 interpreted these results physically using vorticity dynamics arguments. For the double-gyre forcing (1.4), the linear continental slope solution consists of two counterrotating gyres with tails that extend to the southwest corner of the basin ([Fig. 2c](#) of BS97). The subpolar gyre is weaker than the subtropical gyre in part because the subpolar gyre passes through regions of both cyclonic and anticyclonic forcing. The vorticity field given by (1.3b) consists of two dominant vorticity layers aligned along the f/H contours: a negative layer associated with the subtropical gyre and a slightly weaker positive layer associated with the subpolar gyre ([Fig. 2d](#) of BS97). The introduction of inertia leads to the self-advection of these vorticity layers from southwest to northeast and a wrapping of the weaker positive layer around the stronger negative layer at the northern tip of the sheets ([Fig. 3d](#) of BS97). Unsteadiness in the continental slope solutions results from the strong interaction of these vorticity layers.

In contrast, for the flat-bottom basin, the linear solution of (1.3) forced by (1.4) consists of two symmetric counterrotating gyres. The associated vorticity layers also are symmetric and are confined to boundary layers at the western vertical sidewall. These symmetric vorticity layers are well separated from each other in the linear approximation, and BS97 found that these layers did not interact significantly until advection had pulled these layers far offshore. As a result, BS97 found that the solutions of (1.3) for nonzero Ro in a flat-bottom basin showed significantly less eddy formation than the corresponding continental slope solutions.

The double-gyre wind stress curl of (1.4) considered in BS97 corresponds to an x -independent source of positive vorticity in the northern part of the basin and sink in the southern part of the basin so that the net vorticity input from the wind is zero. In the paper, we study solutions of (1.3) for which the single-gyre forcing (1.2) provides a nonzero vorticity input. The wind of (1.2) adds negative vorticity and forces an anticyclonic gyre; we also consider here solutions of (1.3) for wind given by $-(1.2)$ that adds positive vorticity and forces a cyclonic gyre.

As in BS97, vorticity dynamics also provide some insight into the effects of inertia on the single-gyre continental slope solutions of (1.3) forced by the wind (1.2). The vorticity field of the linear, single-gyre continental slope solution consists of a single dominant negative vorticity layer bounded by significantly weaker positive layers ([Fig. 2b](#)). Due to the alignment of these vorticity layers and their asymmetry, strong vorticity interactions are anticipated for the single-gyre continental slope solutions with inertia. In addition, while changing the direction of the wind forcing from anticyclonic to cyclonic only changes the sign of the linear solution of (1.3), numerical experiments reveal that the continental slope solutions with inertia strongly depend upon the sign of the wind forcing. In certain parameter regimes, single-gyre continental slope solutions of (1.3) are unsteady for anticyclonic wind forcing but steady for cyclonic wind forcing. The different behavior exhibited by the continental slope solutions with inertia as the sign of the wind is changed may be interpreted as follows: for anticyclonic winds, the vorticity layers are advected *away* from the southwest corner of the basin where friction is important (where the characteristics intersect the western boundary); therefore, inertial effects are important in regions where damping is ineffective and unsteady, inertially dominated flows are realized. Alternatively, for cyclonic wind forcing, the vorticity layers are advected *into* the southwest corner of the basin where a steady balance between advection, forcing, and damping may be achieved. In contrast, in the flat-bottom basin where friction is important along the western sidewall, steady solutions with inertia are obtained for both anticyclonic and cyclonic winds and are related by the symmetry of the flat-bottom dynamics.

We also find that for single-gyre, cyclonic wind forcing given by $-(1.2)$, multiple equilibria satisfy (1.3) for the basin with the continental slope in certain parameter regimes. In a flat-bottom basin, it recently has been shown that the barotropic vorticity equation (BVE) with lateral friction supports multiple equilibria (e.g., [Ierley and Sheremet 1995](#)) for single-gyre winds although it is speculated there that with linear (Rayleigh) friction, the single-gyre solutions of the BVE are unique. The

question naturally arises as to whether multiple equilibria occur in a basin with a shelf. Here, two steady single-gyre continental slope solutions of (1.3) are found for cyclonic winds above a threshold Rossby number. While only one flat-bottom single-gyre solution branch of (1.3) has been obtained in this study, we have not established whether or not the flat-bottom solutions of (1.3) are unique.

This paper is organized as follows. In [section 2](#), the dynamics and numerical model are briefly described (a more thorough description may be found in BS97). In [section 3](#), the numerical solutions of (1.3) are discussed for anticyclonic and cyclonic single-gyre winds and for the two topographies, the flat-bottom basin, and the basin with the western continental shelf. The numerical results for anticyclonic single-gyre wind forcing are consistent with those obtained in BS97 for double-gyre wind forcing; the introduction of a western continental shelf results in unsteady inertial solutions while the corresponding solutions in a flat-bottom basin are steady. For cyclonic forcing, however, steady solutions are obtained for both topographies in certain parameter regimes. The regions where friction is important are shown to have a significant effect on these solutions.

2. Dynamics and numerical method

As in BS97, we consider a uniform density ocean governed by the hydrostatic primitive equations,

$$\frac{D\mathbf{u}}{Dt} + f\mathbf{k} \times \mathbf{u} = -\nabla\phi - R\mathbf{u} + \frac{\Delta\tau}{H}, \quad (2.1)$$

$$0 = -\frac{\partial\phi}{\partial z} \quad (2.2)$$

$$\nabla \cdot \mathbf{u} + \frac{\partial w}{\partial z} = 0. \quad (2.3)$$

Here, \mathbf{u} , the horizontal part of the velocity (\mathbf{u}, w), is assumed to be z independent; $f = \beta y$ is the Coriolis parameter; \mathbf{k} is the vertical unit vector; $\nabla = (\partial_x, \partial_y)$ is the horizontal gradient operator; ϕ is the pressure (divided by the uniform density); $\Delta\tau = \tau_s - \tau_b$ is the difference between the prescribed stress at the surface and bottom of the ocean; and

$$\frac{D}{Dt} = \frac{\partial}{\partial t} + \mathbf{u} \cdot \nabla.$$

The constant R in [\(2.1\)](#) is the coefficient of Rayleigh friction and the stress terms have been approximated in a manner consistent with the assumption of z -independent horizontal velocity. The boundary conditions on [\(2.1–3\)](#) are no normal flow through the bottom,

$$w = -\mathbf{u} \cdot \nabla H \quad \text{at} \quad z = -H(x, y), \quad (2.4)$$

and rigid lid,

$$w = 0 \quad \text{at} \quad z = 0. \quad (2.5)$$

Introducing the transport streamfunction ψ ,

$$H\mathbf{u} = (-\psi_y, \psi_x), \quad (2.6)$$

which follows from [\(2.3\)–\(5\)](#), and taking the curl of the momentum [equations \(2.1\)](#), we obtain

$$\frac{\partial\zeta}{\partial t} + J\left(\psi, \frac{\zeta + \beta y}{H}\right) = -R\zeta + W(x, y), \quad (2.7a)$$

where ζ is given by [\(1.3b\)](#) and

In the present work, we take the W -forcing term to have the simplified form (1.2).

As in BS97, we nondimensionalize (2.7) by scaling (x, y) by L , z by H_0 (a representative ocean depth), \mathbf{u} by U , w by UH_0/L , t by L/U , Φ by $f_0 UL$, and τ by $f_0 H_0 U$ to obtain the nondimensional vorticity equation (1.3).

The numerical model is that used in BS97. Briefly, to solve (1.3), we replace $\partial\psi/\partial t$ by a centered time difference and regard the resulting equation as an elliptic equation for ψ at the new time. The only boundary condition is $d\psi/dt = 0$. We treat the (linear) $J(\psi, y/H)$ -term semi-implicitly and use a two-dimensional generalization of Leonard's (1984) third-order upwind scheme for the (nonlinear) vorticity advection term in (1.3). The resulting equation then is solved by relaxation at each time step.

3. Numerical solutions

We next present the numerical solutions of (1.3) in a square basin on $0 \leq x \leq 1$, $0 \leq y \leq 1$ with the southern boundary corresponding to the equator as a function of the two controlling parameters (Ro, \mathcal{E}) . The boundary condition is $\psi = 0$ at the western, northern, and eastern coastlines and at the equator (where it corresponds to cross-equatorial symmetry of the flow). As in BS97, we focus on two cases of topography. In the first case, the ocean depth $H(x)$ vanishes smoothly at the western boundary, with the idealized shelf and slope depicted in Figs. 1a,b; the northern and eastern boundaries remain vertical. In the second case, the ocean bottom is flat ($H = 1$) and all coastal boundaries are vertical walls. The dependence of the solutions of (1.3) on the sign of the wind forcing also is examined. The wind of (1.2) forces an anticyclonic circulation; reversing the sign of (1.2) yields cyclonic forcing.

a. Anticyclonic winds

We first describe the solutions of (1.3) for the anticyclonic wind forcing (1.2) as a function of Ro for the fixed value of $\mathcal{E} = 0.01$. The effects of inertia on the flat-bottom solution of (1.3) (Figs. 2c,d) have been established previously (e.g., Veronis 1966). We confirm that a sequence of steady solutions similar to those of Fig. 12 of Veronis (1966) satisfies (1.3) as the Rossby number is increased.¹ Briefly, inertia causes the vorticity layer at the western boundary to be advected northward and then eastward along the northern boundary.

The results of BS97 for a double-gyre wind suggest that continental slope solutions with inertia will be unsteady. As discussed in the introduction, for nonzero Ro , the vorticity layers of the linear continental slope solution are advected away from the southwest corner of the basin where friction is important. Hence, the interaction between the strongly asymmetric vorticity layers of the linear single-gyre solution (Fig. 2b) occurs on the shelf where frictional effects are too weak to establish a steady dynamical balance. As anticipated, unsteady continental slope solutions are obtained for all values of Ro tested ($1.0 \times 10^{-4} \leq \text{Ro} \leq 14 \times 10^{-4}$) for the anticyclonic single-gyre wind (1.2).

We next describe the behavior of the unsteady, anticyclonic single-gyre continental slope solutions as the Rossby number is increased. For small values of Ro ($1.0 \times 10^{-4} \leq \text{Ro} \leq 6.0 \times 10^{-4}$), the landward edge of the tail of the linear anticyclonic gyre is drawn up parallel to the western boundary and small-scale eddying occurs over the shelf. This eddying initiates near the southern end of the vortex layers (Fig. 3). By $\text{Ro} = 8.0 \times 10^{-4}$, the unsteadiness resembles more closely that of the double-gyre solutions of BS97 with meanders in the current jet along the northern edge of the gyre. Figure 4 presents five snapshots of this time-dependent solution for $\text{Ro} = 8.0 \times 10^{-4}$. The vorticity plots show that the nonlinear flow still appears to be influenced by the characteristics of the linear dynamics as the vorticity layers appear to be drawn along both the characteristics that intersect the northern boundary and those that turn toward the interior and intersect the eastern boundary (Fig. 1c).

b. Cyclonic winds

As in the previous subsection, we first describe the solutions of (1.3) for the cyclonic wind forcing $-(1.2)$ as a function of Ro for the fixed value of $\mathcal{E} = 0.01$. The linear flat-bottom solution of (1.3) for cyclonic wind forcing differs from that in Figs. 2c,d only by a sign change (not shown). While Veronis (1966) did not study the effects of inertia on the flat-bottom solution for cyclonic winds, we find that for cyclonic forcing, a sequence of steady solutions satisfy (1.3) as the Rossby number is increased that are related to those for anticyclonic forcing by the symmetry of the flat-bottom dynamics. Figures 5a,b present a flat-bottom solution for $\text{Ro} = 8.0 \times 10^{-4}$ that shows that the (positive) vorticity layer at the

western boundary has been advected southward and then eastward along the equator.

In the linear approximation, reversing the sign of the wind (1.2) simply reverses the sign of the solution of (1.3) for both the flat-bottom and continental slope topography. For both topographies, friction becomes important where the wind-driven flow crosses characteristics; this occurs near where these characteristics intersect the western boundary. In contrast to the flat-bottom topography, however, the characteristics for the continental slope topography intersect the western boundary at a point in the southwest corner of the basin. This has important implications for the effects of inertia on the cyclonic continental slope solutions.

We next describe the continental slope solutions of (1.3) for cyclonic wind forcing as a function of Ro for fixed $\mathcal{E} = 0.01$. For small values of Ro (e.g., $Ro = 2.0 \times 10^{-4}$), the solution of (1.3) is unsteady. Inertia has resulted in the advection of the vorticity layers to the southwest and upon reaching the equator, the flow is drawn along the equator to near the edge of the shelf. The unsteadiness appears as slight oscillations in this flow along the equator. For a range of larger values of Ro , two continental slope solutions of (1.3) are obtained for the same values of the controlling parameters. Above a threshold Ro , these solutions are steady and depend upon the initial conditions.

Figures 5c,d show a steady continental slope solution of (1.3) for $Ro = 8.0 \times 10^{-4}$ starting from a nonzero state. The initial condition for Figs. 5c,d is the solution of (1.3) for $Ro = 7.0 \times 10^{-4}$ starting from rest. We followed this solution for $4.0 \times 10^{-4} \leq Ro \leq 14.0 \times 10^{-4}$. For $Ro = 3.0 \times 10^{-4}$, this solution is unsteady and resembles that described above for $Ro = 2.0 \times 10^{-4}$. In the parameter range where this continental slope solution is steady, the effect of the shelf is to shelter the western boundary from the southward flowing current, but otherwise, this solution resembles the corresponding flat-bottom solution (Figs. 5a,b). Here, inertia advects the vorticity layers across the shelf along the equator.

Figures 6a,b show another steady continental-slope solution of (1.3) for $Ro = 8.0 \times 10^{-4}$ starting from rest. This solution resembles the linear continental slope solution presented in Figs. 6c,d for comparison, but the effects of inertia are evident. First, inertia has caused the southward boundary current to flow more nearly parallel to the western boundary; this effect of inertia also is evident in the unsteady anticyclonic solutions of Fig. 4 where the northward boundary current flows parallel to the western coastline. Second, inertia has caused the flow along the seaward edge of the shelf to overshoot the latitude where the flow in the linear approximation is returned to the interior. Starting from the solution in Figs. 6a,b, we followed this solution branch for $3.0 \times 10^{-4} \leq Ro \leq 10.0 \times 10^{-4}$. For larger values of Ro , the solution of (1.3) jumps to the other solution branch described above (e.g., Figs. 5c,d).

An important difference between the two steady continental shelf solutions of Figs. 5c,d and 6a,b is the region where dissipation is effective. For the solution of Figs. 5c,d, the flow overshoots the edge of the shelf and a boundary layer forms along the equator. Contour plots of the individual terms in (1.3) show that damping and inertia are dominant in this boundary layer. Above a threshold Rossby number of $Ro \approx 3.0 \times 10^{-4}$ for $\mathcal{E} = 0.01$, this solution is steady and closely resembles the corresponding flat-bottom solution with inertia (Figs. 5a,b). In contrast, for the second solution shown in Figs. 6a,b, contour plots of the individual terms in (1.3) reveal that strong dissipative effects are localized in the southwest part of the basin. Above a threshold Rossby number of $Ro \approx 2.0 \times 10^{-4}$ for $\mathcal{E} = 0.01$, a steady balance between inertia and this localized dissipation is achieved. This solution depends strongly upon the shelf topography with a structure that resembles that of the linear continental slope solution (Fig. 6c,d) and the f/H contours (Fig. 1c).

4. Remarks

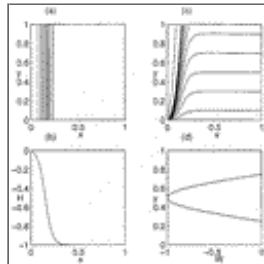
Highly idealized models of the general circulation such as (1.3) are useful in lending insight to more realistic general circulation models and many of the theoretical studies to date have focused on flat-bottom models. The results presented here indicate that a western continental slope has a significant effect on the inertial solutions of this simple model. The present solutions of (1.3) for the single-gyre wind stress curl, (1.2), complement the solutions of BS97 for the double-gyre wind stress curl, (1.4). In particular, the present results show that whether frictional effects are localized regionally or in boundary layers at vertical sidewalls significantly affects the model solutions. A future study will examine how baroclinicity affects these model results.

Acknowledgments

I thank Rick Salmon for valuable discussions. I also thank the reviewers for helpful comments. This work was supported by NSF-OCE-9633057.

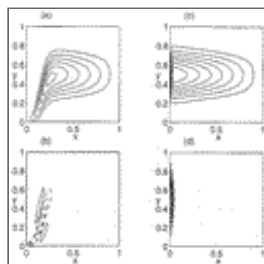
- Becker, J. M., and R. Salmon, 1997: Eddy formation over a continental slope. *J. Mar. Res.*, **55**, 181–200..
- Cummins, P. F., 1992: Inertial gyres in decaying and forced geostrophic turbulence. *J. Mar. Res.*, **50**, 545–566..
- Irley, G. R., and V. A. Sheremet, 1995: Multiple solutions and advection-dominated flows in the wind-driven circulation. Part I: Slip. *J. Mar. Res.*, **53**, 703–737..
- Kubokawa, A., and J. C. McWilliams, 1996: Topographic ocean gyres: A western boundary slope. *J. Phys. Oceanogr.*, **26**, 1468–1479..
[Find this article online](#)
- Leonard, B. P., 1984: Third-order upwinding as a rational basis for computational fluid dynamics. *Computational Techniques and Applications: CTAC-83*, J. Noye and C. Fletcher, Eds., Elsevier, 106–120..
- Munk, W. H., 1950: On the wind-driven ocean circulation. *J. Meteor.*, **7**, 79–93..
- Rhines, P. B., and W. R. Young, 1983: How rapidly is a passive scalar mixed within closed streamlines? *J. Fluid Mech.*, **133**, 133–145..
- Salmon, R., 1992: A two-layer Gulf Stream over a continental slope. *J. Mar. Res.*, **50**, 341–365..
- , 1994: Generalized two-layer models of ocean circulation. *J. Mar. Res.*, **52**, 865–908..
- Stommel, H., 1948: The westward intensification of wind-driven ocean currents. *Trans. Amer. Geophys. Union*, **29**, 202–206..
- Veronis, G., 1966: Wind-driven ocean circulation-Part 2. Numerical solution of the nonlinear problem. *Deep-Sea Res.*, **13**, 30–55..
- Welander, P., 1968: Wind-driven circulation in one- and two-layer oceans of variable depth. *Tellus*, **20**, 1–16..

Figures



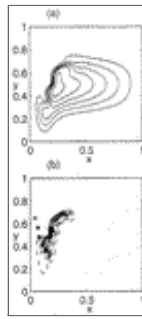
[Click on thumbnail for full-sized image.](#)

Fig. 1. (a),(b) The ocean depth $H(x, y)$, which varies from zero at the western coast to 1 in the interior. (c) The corresponding contours of y/H . (d) The anticyclonic wind stress curl, (1.2).



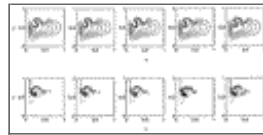
[Click on thumbnail for full-sized image.](#)

Fig. 2. A steady, linear circulation. The transport streamfunction Ψ (upper panels) and vorticity multiplied by the ocean depth $H\xi$ (lower panels) that satisfy (1.3) with $(Ro, \mathcal{E}) = (0.0, 0.01)$; with wind stress curl given by (1.2) and (a),(b) a basin with a western shelf; the $H(x, y)$ of [Figs. 1a,b](#), and (c),(d) a flat-bottom basin with $H(x, y) = 1$. In the continental slope solution (b), a single dominant negative vorticity sheet is bounded by weaker positive layers. In contrast, for the flat-bottom solution (d), the vorticity sheet lies in the frictional western boundary layer. We present contours of $H\xi$ rather than ξ because of the large values of vorticity that occur in the southwest corner of the basin in the continental slope solutions. In all contour plots, the solid (dashed) contours correspond to positive (negative) values and the contour intervals for Ψ and $H\xi$ are 0.1 and 100, respectively.



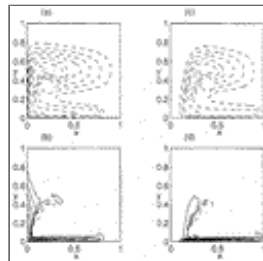
Click on thumbnail for full-sized image.

Fig. 3. Unsteady continental slope solution for anticyclonic forcing. Snapshot of ψ (upper panels) and $H\zeta$ (lower panels) that satisfy (1.3) for $(Ro, \mathcal{E}) = (2.0 \times 10^{-4}, 0.01)$, the wind stress curl (1.2), and $H(x, y)$ of Figs. 1a,b.



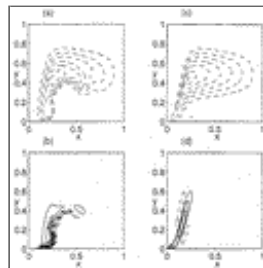
Click on thumbnail for full-sized image.

Fig. 4. Unsteady continental slope solutions for anticyclonic forcing. Snapshots of ψ (upper panels) and $H\zeta$ (lower panels) that satisfy (1.3) for $(Ro, \mathcal{E}) = (8.0 \times 10^{-4}, 0.01)$, the wind stress curl (1.2), and $H(x, y)$ of Figs. 1a,b. Time increases from left to right.



Click on thumbnail for full-sized image.

Fig. 5. A steady flat-bottom solution and a steady continental slope solution for cyclonic forcing. The transport stream function ψ (upper panels) and vorticity multiplied by the ocean depth $H\zeta$ (lower panels) that satisfy (1.3) with the wind stress curl given by $-(1.2)$ and (a),(b) $(Ro, \mathcal{E}) = (8.0 \times 10^{-4}, 0.01)$, and $H(x, y) = 1$ and (c),(d) $(Ro, \mathcal{E}) = (8.0 \times 10^{-4}, 0.01)$ and the $H(x, y)$ of Figs. 1a,b. The solution in (c),(d) was obtained starting from a nonzero state described in the text.



Click on thumbnail for full-sized image.

Fig. 6. Steady continental slope solutions for cyclonic forcing. The transport stream function ψ (upper panels) and vorticity multiplied by the ocean depth $H\zeta$ (lower panels) that satisfy (1.3) with $H(x, y)$ of Figs. 1a,b; the wind stress curl given by $-(1.2)$ and (a),(b) $(Ro, \mathcal{E}) = (8.0 \times 10^{-4}, 0.01)$, and (c),(d) $(Ro, \mathcal{E}) = (0.0, 0.01)$. The solution in (a) (b) was obtained starting from rest.

¹ Veronis (1966) considered a wind stress curl confined to the lower $\frac{3}{4}$ of the basin, while the wind stress curl (1.2) is confined to the middle half of the present model basin.

Corresponding author address: Dr. Janet M. Becker, Dept. of Geology and Geophysics, University of Hawaii, 1680 East-West Road, Honolulu, HI 96822.

E-mail: jbecker@soest.hawaii.edu

[top](#) ▲



© 2008 American Meteorological Society [Privacy Policy and Disclaimer](#)
Headquarters: 45 Beacon Street Boston, MA 02108-3693
DC Office: 1120 G Street, NW, Suite 800 Washington DC, 20005-3826
amsinfo@ametsoc.org Phone: 617-227-2425 Fax: 617-742-8718
[Allen Press, Inc.](#) assists in the online publication of *AMS* journals.